

## Photoswitchable Dihydroazulene Macrocycles for Solar Energy Storage: The Effects of Ring Strain

Alexandru Vlasceanu, Benjamin Normann Frandsen, Anders B. Skov, Anne Schou Hansen, Mads Georg Rasmussen, Henrik Grum Kjaergaard, Kurt V. Mikkelsen, and Mogens Brøndsted Nielsen

*J. Org. Chem.*, **Just Accepted Manuscript** • DOI: 10.1021/acs.joc.7b01760 • Publication Date (Web): 30 Aug 2017

Downloaded from <http://pubs.acs.org> on August 30, 2017

### Just Accepted

“Just Accepted” manuscripts have been peer-reviewed and accepted for publication. They are posted online prior to technical editing, formatting for publication and author proofing. The American Chemical Society provides “Just Accepted” as a free service to the research community to expedite the dissemination of scientific material as soon as possible after acceptance. “Just Accepted” manuscripts appear in full in PDF format accompanied by an HTML abstract. “Just Accepted” manuscripts have been fully peer reviewed, but should not be considered the official version of record. They are accessible to all readers and citable by the Digital Object Identifier (DOI®). “Just Accepted” is an optional service offered to authors. Therefore, the “Just Accepted” Web site may not include all articles that will be published in the journal. After a manuscript is technically edited and formatted, it will be removed from the “Just Accepted” Web site and published as an ASAP article. Note that technical editing may introduce minor changes to the manuscript text and/or graphics which could affect content, and all legal disclaimers and ethical guidelines that apply to the journal pertain. ACS cannot be held responsible for errors or consequences arising from the use of information contained in these “Just Accepted” manuscripts.

# Photoswitchable Dihydroazulene Macrocycles for Solar Energy Storage: The Effects of Ring Strain

Alexandru Vlasceanu, Benjamin N. Frandsen, Anders B. Skov, Anne Schou Hansen, Mads Georg Rasmussen, Henrik G. Kjaergaard, Kurt V. Mikkelsen, Mogens Brøndsted Nielsen\*

Department of Chemistry, Center for Exploitation of Solar Energy, University of Copenhagen, Universitetsparken 5, DK-2100 Copenhagen Ø, Denmark. E-mail: mbn@chem.ku.dk

*Keywords: electrocyclic reactions, energy conversion, macrocycles, photochromism, strained molecules*

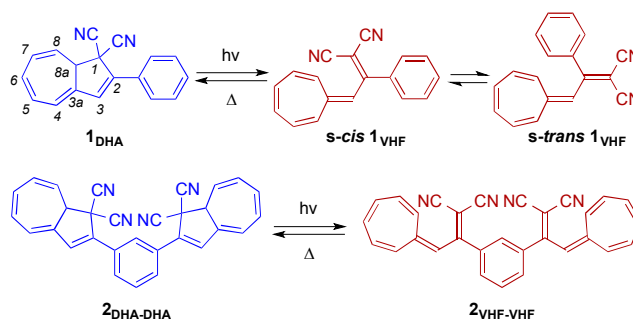
**ABSTRACT:** Efficient energy storage and release are two major challenges of solar energy harvesting technologies. The development of molecular solar thermal systems presents one approach to address these issues by tuning the isomerization reactions of photo-/thermoswitches. Here we show that the incorporation of photoswitches into macrocyclic structures is a particularly attractive solution for increasing the storage time. We present the synthesis and properties of a series of macrocycles incorporating two dihydroazulene (DHA) photoswitching subunits, bridged by linkers of varying chain length. Independent of ring size, all macrocycles exhibit stepwise, light-induced, ring-opening reactions (DHA-DHA to DHA-VHF to VHF-VHF; VHF = vinylheptafulvene) with the first DHA undergoing isomerization with a similar efficiency as the uncyclized parent system while the second (DHA-VHF to VHF-VHF) is significantly slower. The energy-releasing, VHF-to-DHA, ring closures also occur in a stepwise manner and were systematically found to proceed slower in the more strained (smaller) cycles, but in all cases with a remarkably slow conversion of the second VHF to DHA. We managed to increase the half-life of the second VHF-to-DHA conversion from 65 h to 202 h at room temperature by simply decreasing the ring size. A computational study reveals the smallest macrocycle to have the most energetic VHF-VHF state and hence highest energy density.

## Introduction

Molecular photoswitches are attractive entities for the development of advanced functional nanostructures and materials such as optical data storage devices, logic gates, and sensors, as well as for control of biological systems.<sup>1</sup> The dihydroazulene/vinylheptafulvene molecular photo/thermoswitch (**1<sub>DHA</sub>**/**1<sub>VHF</sub>**; Scheme 1) can undergo a 10- $\pi$  electrocyclic reaction where significant structural changes occur upon the ring opening/closure reactions.<sup>1f,2</sup> This system has also been recently identified as a possible material on which to base molecular solar-thermal (MOST) energy storage technologies.<sup>3</sup> Currently, the major challenges for the exploitation of solar energy are its efficient capture, storage, and on-demand release. MOST systems take advantage of the photoactive nature of certain chemical compounds, and although real applications have not yet matured, fundamental structure-property relationships have been established for various systems as well as promising proof-of-concept demonstration set-ups.<sup>3,4</sup> Solar energy absorption by such materials is accompanied by a photochemical isomerization forming a high-energy photoisomer, hence converting incident radiant energy into chemical energy (Figure 1). In the case of electrocyclic reactions, this energy is stored in the formation of bonds between atoms, which can be subsequently broken to release the energy as heat. The DHA-VHF couple is particularly attractive for such “closed cycle” thermal fuels (involving

no CO<sub>2</sub> emissions) as only the DHA-to-VHF conversion is induced by light. Light harvesting in this manner generates the meta-stable VHF isomer, which represents an energy reservoir that discharges in time.

**Scheme 1. Photo/thermal switching of the parent **1<sub>DHA</sub>**/**1<sub>VHF</sub>** and dimeric **2<sub>DHA-DHA</sub>**/**2<sub>VHF-VHF</sub>** systems. The commonly used numbering scheme is indicated.**



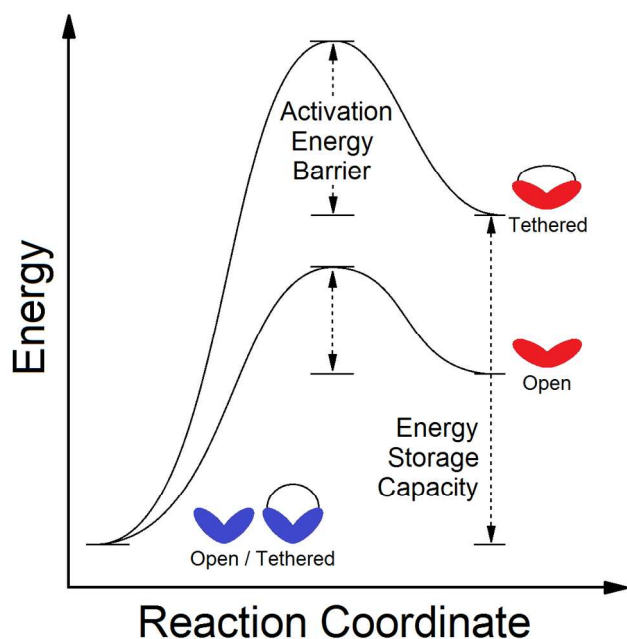


**Figure 1.** Simplified potential energy surface for acyclic and cyclic, dimeric systems converting between DHA-DHA (blue) and VHF-VHF (red) isomers.

Two major challenges for MOST systems to be effective are achieving a sufficiently high energy storage capacity and control over the energy discharge. Taking various considerations into account, the maximum energy density of a solar-thermal battery based on the isomerization of an organic system has been estimated to be limited to ca.  $1 \text{ MJ kg}^{-1}$  (depending, however, on the absorption maximum of the photoswitch).<sup>4c</sup> This energy storage capacity corresponds to that of the unsubstituted norbornadiene-quadracyclane (NB/QC) system.<sup>4a</sup>

Although the efficiency of the photo-induced ring opening has been found to be generally quite high for many DHAs (photoisomerization of  $1_{\text{DHA}}$  occurs with a quantum yield of 55%<sup>2b</sup>), calculations<sup>3a</sup> estimate that the energy density of the parent  $1_{\text{DHA}}/1_{\text{VHF}}$  system lies at ca.  $0.11 \text{ MJ kg}^{-1}$ . In addition, the half-life ( $1_{\text{VHF}} t_{1/2} = 218 \text{ min}$  in MeCN<sup>5</sup>) of the thermal discharge is too low with regard to practical applications, at least in a liquid medium (e.g. heat transfer fluids of concentrated solar power plants).

Computational work by Durgun and Grossman<sup>4d</sup> on azobenzenes<sup>6</sup> and recent experimental results from our lab<sup>3b</sup> on DHAs have suggested that the incorporation of photoactive moieties into strained macrocyclic systems could be a viable strategy towards increasing the Gibbs free energy between the light-harvesting DHA and metastable VHF states as well as providing a method for controlling the energy release (Figure 1). Established kinetic/thermodynamic postulates (*i.e.* Bell-Evans-Polanyi principle<sup>7</sup>), however, imply that increasing the relative energy difference between the two states will also undesirably result in a lower activation energy for the exothermic back reaction (VHF  $\rightarrow$  DHA). Nevertheless, our recent report<sup>3b</sup> has indicated that incorporating

two VHF units in a macrocycle presents an alternative approach by providing energy discharge on two time-scales *via* an initially fast VHF ring closure followed by a slower one. If designed properly, the overall heat release could be larger than for a non-tethered system although the second, slow discharging may still be of lower energy than the first. One important property of the DHA-VHF system remains the pre-equilibrium between *s-cis* and *s-trans* conformers of VHF. While the *s-trans* conformer is usually more thermodynamically stable, only the *s-cis* conformer has the geometry needed for ring closure. Tuning the position of this equilibrium towards the *s-trans* conformer, possibly via constraints imposed by macrocyclic structures, may be a convenient tool for enhancing the lifetime of the VHF in spite of a smaller activation energy for the *s-cis* conformer's ring closure reaction.

Here we set out to conduct a more comprehensive investigation of the influence of macrocyclic ring strain on the thermodynamic and kinetic properties of the DHA/VHF system. This was undertaken through the synthesis and characterization of three macrocyclic systems ( $3_{\text{DHA-DHA}}$ ,  $4_{\text{DHA-DHA}}$ , and  $5_{\text{DHA-DHA}}$ ; Figure 2), varying only in the length of the bridging unit connecting the two ends of the dimeric  $2_{\text{DHA-DHA}}$  system shown in Scheme 1. Compound  $2_{\text{DHA-DHA}}$  can be easily accessed<sup>8</sup> and was recently shown to be a convenient precursor for  $4_{\text{DHA-DHA}}$ .<sup>3b</sup> Here we show how this route can be generalized to allow the synthesis of macrocycles of various sizes.

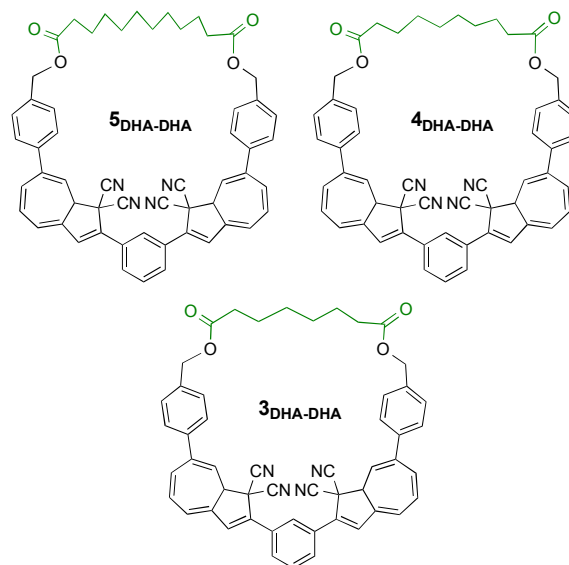


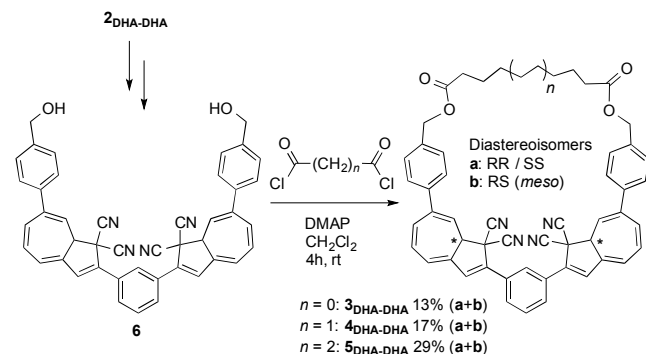
**Figure 2.** Target macrocycles  $3_{\text{DHA-DHA}}$ ,  $4_{\text{DHA-DHA}}$ , and  $5_{\text{DHA-DHA}}$ .

## Results and Discussion

**Synthesis and Characterization.** The syntheses of the three macrocyclic DHA systems are shown in Scheme 2. In each case, we start from the known diol  $6$ ,<sup>3b</sup> which is readily made via two Suzuki couplings on the dibromosubstituted derivative of  $2_{\text{DHA-DHA}}$ . As previously described, diol  $6$  is difficult to obtain pure, as it is unstable to column chromatography.<sup>3b</sup> Each of the three macrocyclic DHA systems ( $3_{\text{DHA-DHA}}$ ,  $4_{\text{DHA-DHA}}$ , and  $5_{\text{DHA-DHA}}$ )

exists as a pair of diastereoisomers (**a/b**), the synthesis and purification of which could be accomplished in a similar way to that recently reported. The previously reported synthesis conditions involve slow, yet simultaneous addition of two solutions (diol **6** and a diacyl chloride) to a third solution of pyridine in  $\text{CH}_2\text{Cl}_2$ , which was then stirred overnight at rt.<sup>3b</sup> Minor changes in the synthesis of the key macrocyclization step could be achieved using *N,N*-dimethylaminopyridine (DMAP) to promote the diester formation, reducing the reaction time from overnight to only a few hours. The macrocycles were separated from any byproducts (presumably including oligomers) by column chromatography on silica gel using 1% acetic acid in toluene as eluent. Minor impurities, which seemed to be macrocyclic azulene byproducts resulting from elimination of HCN, were subsequently removed by size exclusion chromatography. An increase in flexibility with increasing ring size (**3**<sub>DHA-DHA</sub> to **4**<sub>DHA-DHA</sub> to **5**<sub>DHA-DHA</sub>) seems to be reflected in the yields of the macrocyclization reactions; 13% (**3ab**), 17% (**4ab**), and 29% (**5ab**). It is also interesting to note that the melting points<sup>9</sup> of the small macrocycles **3a** and **3b** are higher than those of the large macrocycles **5a** and **5b** (**3a**<sub>DHA-DHA</sub>: 150-155 °C; **4a**<sub>DHA-DHA</sub>: 138-150 °C; **5a**<sub>DHA-DHA</sub>: 131-136 °C; **3b**<sub>DHA-DHA</sub>: 156-163 °C; **4b**<sub>DHA-DHA</sub>: 160-166 °C; **5b**<sub>DHA-DHA</sub>: 128-134 °C), but for all compounds quite broad ranges are obtained.

**Scheme 2. Synthesis of macrocycles 3<sub>DHA-DHA</sub>, 4<sub>DHA-DHA</sub>, and 5<sub>DHA-DHA</sub> as pairs of diastereoisomers a/b.**



Although single crystals could be grown from solutions of the macrocycles presented here, only few samples were suitable for X-ray diffraction (Figure 3). Furthermore, even these exhibited conformational disorder and although the dimeric DHA moieties are well resolved, the overall structures could not be sufficiently optimized due to considerable disorder in the bridging alkyl chain and encapsulated solvent molecules. The structures do still provide evidence for increased ring strain with decreasing macrocycle size as can be observed in a rather “loose” conformation of **5**<sub>DHA-DHA</sub> compared to the more “taut” **4**<sub>DHA-DHA</sub><sup>3b</sup> and **3**<sub>DHA-DHA</sub>, which clearly exhibits a strained, “sling-shot” conformation in its structure.

Differences in ring strain might also be expected to distort/shift the interatomic stretching/bending vibrations of these cycles; however, IR (ATR) spectroscopy shows no effective differences in the intensities or shifts of the absorptions. For comparison, carbonyl (C=O and C-O) stretches overlap nearly perfectly in both diastereoisomers

of all three cycles **3**<sub>DHA-DHA</sub> (1732; 1160  $\text{cm}^{-1}$ ), **4**<sub>DHA-DHA</sub> (1732; 1163  $\text{cm}^{-1}$ ), and **5**<sub>DHA-DHA</sub> (1730; 1162  $\text{cm}^{-1}$ ).

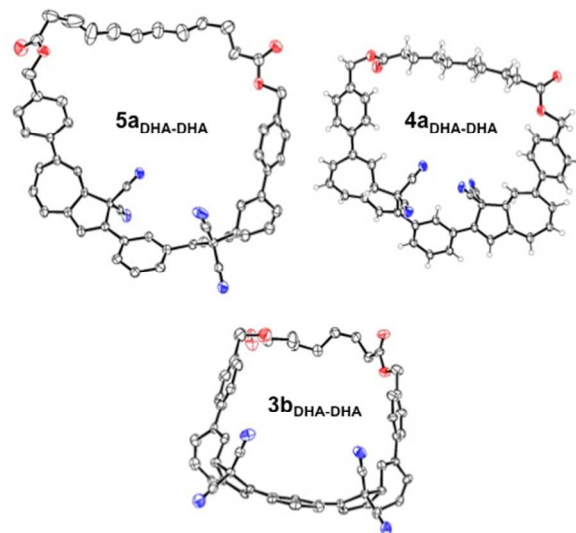


**Figure 3.** Molecular structures of macrocycles **3b**<sub>DHA-DHA</sub> (CCDC 1570242), **4a**<sub>DHA-DHA</sub> (CCDC 1450505), and **5a**<sub>DHA-DHA</sub> (CCDC 1570243). Hydrogen atoms were omitted in the optimizations of **3b**<sub>DHA-DHA</sub> and **5a**<sub>DHA-DHA</sub>. Thermal ellipsoids are shown at 50% probability level. Single crystals were grown from  $\text{CHCl}_3$ /heptane (**3b**<sub>DHA-DHA</sub>) or  $\text{CHCl}_3$ /EtOH (**4a**<sub>DHA-DHA</sub>, **5a**<sub>DHA-DHA</sub>). Solvent molecules were removed for clarity. Full asymmetric units are shown in SI.

The <sup>1</sup>H- and <sup>13</sup>C-NMR spectra of all macrocycles are completely consistent with their structures. All protons in the core DHA dimer seem slightly but consistently shifted downfield with increasing macrocycle size for both diastereoisomers,  $\delta$  **3**<sub>DHA-DHA</sub> < **4**<sub>DHA-DHA</sub> < **5**<sub>DHA-DHA</sub>. The same trend is observed for the <sup>13</sup>C-NMR resonances of the carbonyl carbon atoms. The two diastereoisomers **a/b** for each macrocycle can also be distinguished by <sup>1</sup>H- and <sup>13</sup>C-NMR spectroscopies. All <sup>1</sup>H resonances of **3b**<sub>DHA-DHA</sub>, for example, are systematically shifted upfield compared to **3a**<sub>DHA-DHA</sub>. This trend is not as encompassing for the other two macrocycles although most resonances of **b** diastereoisomers are upfield shifted relative those of the **a**'s.

The UV-vis absorption spectra of macrocycles **3a**<sub>DHA-DHA</sub>, **4a**<sub>DHA-DHA</sub>, and **5a**<sub>DHA-DHA</sub> show no substantial differences between the wavelength or intensity of their lowest energy absorptions (Figure 4). All macrocycles exhibit characteristic absorptions assigned to the DHA-DHA moieties at *ca.*  $\lambda_{\text{max}} = 356$  nm exhibiting molar absorptivities around  $\epsilon = 28000$   $\text{M}^{-1}\text{cm}^{-1}$ . As expected, these are approximately twice as large as that of **1**<sub>DHA</sub>, suggesting that the chromophores of the DHA-DHA macrocycles can be considered as a sum of two individual **1**<sub>DHA</sub> units. Furthermore, as all DHA-DHAs present similar molar absorptivities, it can be concluded that these exhibit no significant conformational distortion imposed by cyclic strain, compared to **1**<sub>DHA</sub>, even in the smallest system (**3**), in line with the molecular structures achieved

by X-ray crystallography. The absorptions are, however, slightly broader with increased ring size, observable in both diastereoisomers of **4**<sub>DHA-DHA</sub> and **5**<sub>DHA-DHA</sub> compared to those of **3**<sub>DHA-DHA</sub>. Such broadening could be the result of greater flexibility and degrees of freedom in the larger macrocycles.

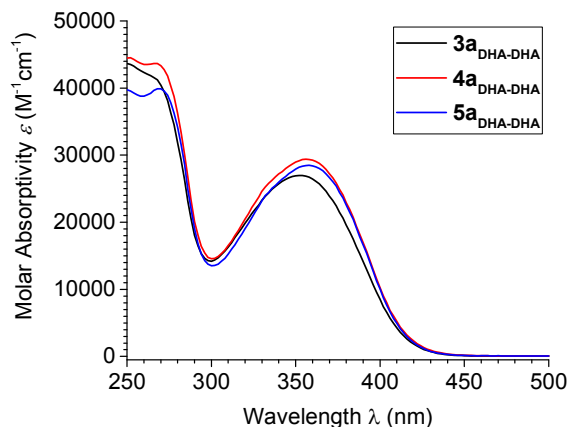


**Figure 4.** Measured UV-Vis absorption spectra of macrocycles **3a**<sub>DHA-DHA</sub>, **4a**<sub>DHA-DHA</sub>, and **5a**<sub>DHA-DHA</sub> in MeCN. Those of **3-5b**<sub>DHA-DHA</sub> are shown in the SI (Fig S21).

Upon photoisomerization of dimer **2**<sub>DHA-DHA</sub> to **2**<sub>VHF-VHF</sub>, it is observed that the molar absorptivity of **2**<sub>VHF-VHF</sub> is roughly double that of monomeric **1**<sub>VHF</sub>.<sup>8</sup> Considering the VHF-VHF states of the strained macrocyclic structures, **3**<sub>VHF-VHF</sub>, **4**<sub>VHF-VHF</sub>, and **5**<sub>VHF-VHF</sub>, however, it is observed (*vide infra*) that the molar absorptivities of the second VHF do not reach nearly the same intensity as would be expected of two independent and non-disturbed VHF chromophores. This indicates that ring strain in these species might be playing a significant role in distorting the structures. Thus far, characterization of the three macrocyclic systems (**3**<sub>DHA-DHA</sub>, **4**<sub>DHA-DHA</sub>, and **5**<sub>DHA-DHA</sub> **a/b**) has indicated that decreasing the length of the diester linker does introduce some ring strain in the DHA-DHA states, although a greater effect is hypothesized in the more conformationally elongated VHF-VHF states.

**Ring Opening Kinetics.** All macrocycles were found to undergo stepwise photoisomerization reactions from DHA-DHA to DHA-VHF to VHF-VHF by irradiation at 356 nm (Scheme 3). This process could easily be followed by UV-Vis absorption spectroscopy by monitoring the emergence of the characteristic VHF absorption at 494 nm (Figure 5). Due to the chiral nature of the DHA moiety, each of the three DHA-DHA macrocycles exists as a pair of diastereoisomers (**a** and **b**), which are in fact observed to exhibit significantly different ring opening kinetics. Upon ring opening of the DHA moieties, however, the chirality is lost resulting in only one pair of enantiomers for the DHA-VHF state and none for the final VHF-VHF state.

The kinetics of the photoisomerization reactions could be modeled by a sum of two exponential functions characterized by two time constants ( $\tau_1$  and  $\tau_2$ ), which, to an approximation, relate to the two individual ring-opening reactions (Scheme 3). To calibrate these time constants

for **3-5a**<sub>DHA-DHA</sub>, the parent **1**<sub>DHA</sub> was also photoisomerized before each macrocyclic system to provide a reference,  $\tau_{ref}$ . The relative ring opening efficiencies can be reasonably approximated by the  $\tau_2/\tau_1$  ratio as well as  $\tau_2/\tau_{ref}$  and  $\tau_1/\tau_{ref}$ . These data are summarized in Table 1.

**Scheme 3. Interconversions between the three different isomers of the macrocyclic systems.**

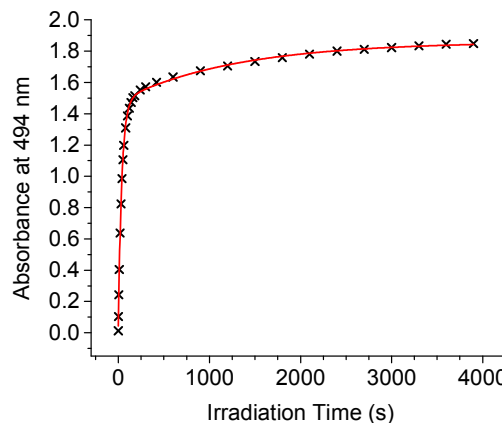
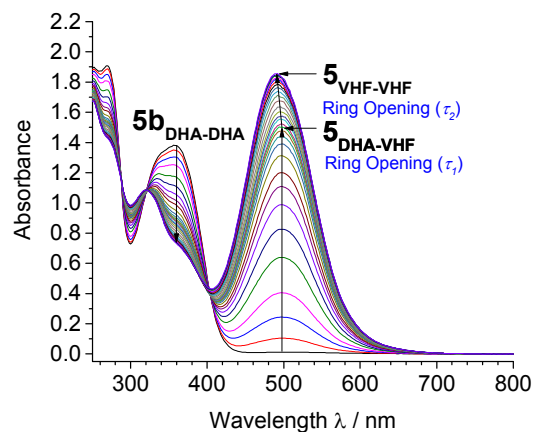
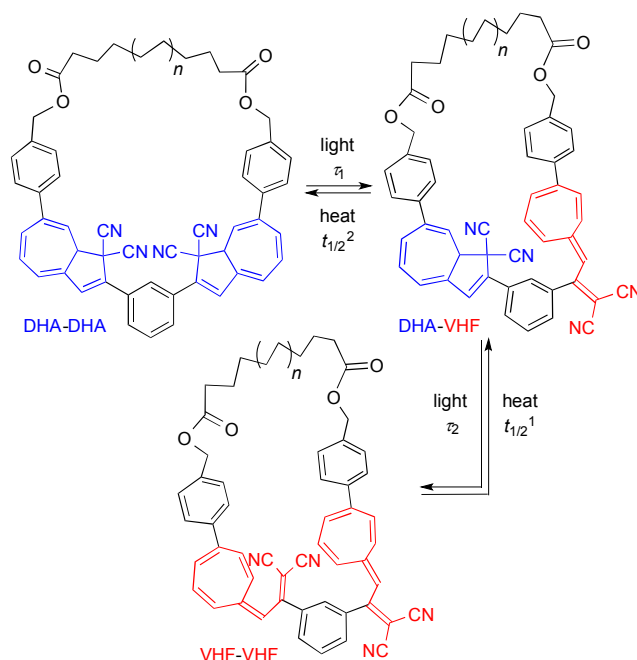


**Figure 5.** Top: Measured UV-Vis absorption spectra showing the photoisomerization of **5b**<sub>DHA-DHA</sub> to **5**<sub>DHA-VHF</sub>

to **5**<sub>VHF-VHF</sub> in MeCN by irradiation at 356 nm. Bottom: Absorbance at  $\lambda = 494$  nm plotted as a function of irradiation time and fitted by a biexponential function (red curve):  $A(t) = c_1 \exp(-t/\tau_1) + c_2 \exp(-t/\tau_2) + A_\infty$ .

**Table 1. Ratios between time constants  $\tau_{\text{ref}}$ ,  $\tau_1$ , and  $\tau_2$  describing the photochemical ring opening reactions of **1**<sub>DHA</sub> (ref) and macrocycles **3**<sub>DHA-DHA</sub>, **4**<sub>DHA-DHA</sub>, and **5**<sub>DHA-DHA</sub>. Values were obtained by fitting the time evolution of the characteristic VHF absorbance by the exponential function:  $A(t) = c_1 \exp(-t/\tau_1) + c_2 \exp(-t/\tau_2) + A_\infty$  as in Figure 5.**

	<b>3a</b>	<b>4a</b>	<b>4b</b>	<b>5a</b>	<b>5b</b>
$\tau_2/\tau_1$	39.2	59.6	34.4	49.4	33.1
$\tau_1/\tau_{\text{ref}}$	0.96	0.75	1.3	0.73	
$\tau_2/\tau_{\text{ref}}$	37.8	44.7	45.6	36.1	

The results reveal that the first ring opening exhibited by all DHA-DHA macrocycles is comparable to that of the **1**<sub>DHA</sub>/**1**<sub>VHF</sub> reference system and also that this first ring opening is significantly faster than the second ( $\tau_1 \ll \tau_2$ ).

**Structural/Spectral Correlations.** Based on a recently published computational and experimental investigation of conformationally distorted DHA/VHF systems, it can be reasonably concluded that a strong correlation exists between the structure of the DHA/VHF chromophores and their respective UV-Vis absorption spectra.<sup>10</sup> Structurally, the characteristic absorptions of **1**<sub>DHA</sub> ( $\lambda_{\text{max}} = 354$  nm,  $\epsilon_{354 \text{ nm}} = 16500 \text{ M}^{-1} \text{ cm}^{-1}$ ) and **s-trans 1**<sub>VHF</sub> ( $\lambda_{\text{max}} = 472$  nm,  $\epsilon_{472 \text{ nm}} = 32000 \text{ M}^{-1} \text{ cm}^{-1}$ ) can be assigned to the HOMO/LUMO transition corresponding to the relatively planar and undisturbed chromophores highlighted in Figure 6 (see SI for details).

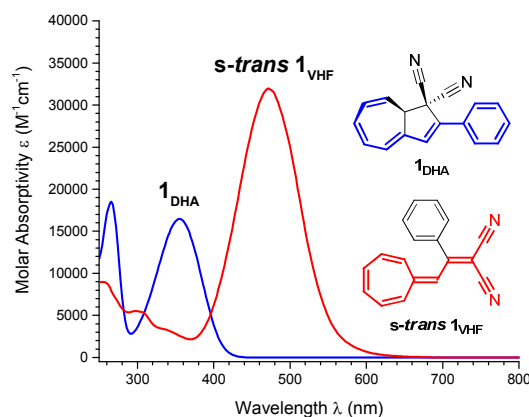


**Figure 6.** Measured UV-Vis spectra of **1**<sub>DHA</sub> (racemic mixture) and **1**<sub>VHF</sub> (*s-cis/s-trans* equilibrium mixture) in MeCN at 25 °C. The chromophores giving rise to the lowest energy absorptions are highlighted in blue for **1**<sub>DHA</sub> and red for **s-trans 1**<sub>VHF</sub> (which is the dominant conformer present).

Structural distortion of the VHF chromophores away from planarity results in poorer  $\pi$ -electron delocalization and thus significantly lower molar absorptivities with slightly blue-shifted  $\lambda_{\text{max}}$  values (Figure S22).<sup>10</sup> The *s-cis* VHF chromophore is also calculated to exhibit a lower molar absorptivity, again likely a result of poorer  $\pi$ -conjugation due to non-planarity. Compared to the more rigid DHAs, the VHF chromophores seem to be more prone to conformational distortion due to their greater flexibility. Computational models of the HOMO and LUMO orbitals of the DHA and *s-trans* VHF isomers are presented in the SI (Figure S27).

Upon photochemical ring opening of the macrocyclic DHA-DHAs, the DHA-VHF isomers are consistently observed to exhibit molar absorptivities of ca.  $\epsilon_{356 \text{ nm}} \approx 19000 \text{ M}^{-1} \text{ cm}^{-1}$  and  $\epsilon_{498 \text{ nm}} \approx 32000 \text{ M}^{-1} \text{ cm}^{-1}$ . By considering the two DHA and VHF chromophores independently, it is observable that the absorption spectrum of DHA-VHF resembles that obtained by adding the absorptions of **1**<sub>DHA</sub> ( $\epsilon_{354 \text{ nm}} = 16500 \text{ M}^{-1} \text{ cm}^{-1}$ ) and **s-trans 1**<sub>VHF</sub> ( $\epsilon_{472 \text{ nm}} = 32000 \text{ M}^{-1} \text{ cm}^{-1}$ ) as shown in Figure 7. This comparison serves to suggest that the core macrocyclic DHA-VHF structure can be approximated by one structurally undisturbed **1**<sub>DHA</sub> chromophore and a planar, relatively undistorted **s-trans 1**<sub>VHF</sub> chromophore.

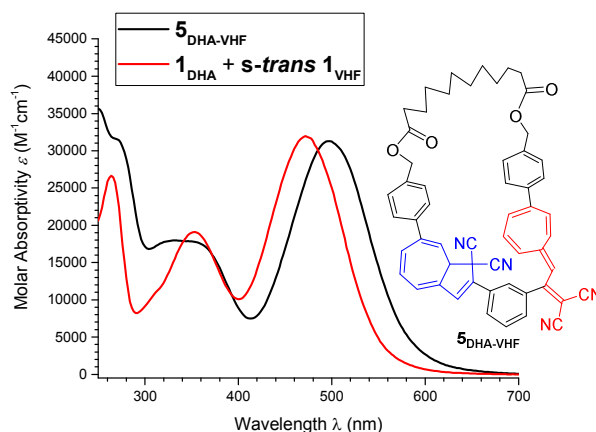


**Figure 7.** Measured molar absorptivities of **5**<sub>DHA-VHF</sub> and a sum of **1**<sub>DHA</sub> + **s-trans 1**<sub>VHF</sub> as a function of wavelength in MeCN. Also shown is a representation of a possible **5**<sub>DHA-VHF</sub> structure giving rise to the **5**<sub>DHA-VHF</sub> spectrum.

Notably, the second ring opening reaction from DHA-VHF to VHF-VHF results in only a small VHF absorptivity increase as well as a slight blueshift of the  $\lambda_{\text{max}}$  to 492 nm ( $\epsilon \approx 37000 \text{ M}^{-1} \text{ cm}^{-1}$ ). Concurrently, the DHA absorption at 360 nm is also observed to decrease only slightly (Figure 8, top). Structurally, ring opening of the second DHA moiety to VHF is hypothesized to result in increased cyclic strain which is alleviated through conformational distortion in one of the two VHF units. The resulting VHF-VHF structure may thus be approximated by one VHF maintaining an *s-trans* conformation and another exhibiting a structurally distorted and likely *s-cis* VHF conformation (*vide infra*).

Considering **s-trans 7**<sub>VHF</sub> as a model system for a distorted VHF moiety, it becomes reasonable that only a

small absorptivity increase is observed for the characteristic VHF-VHF absorption of the macrocyclic structures (Figure 8). Furthermore, calculations predict a higher molar absorptivity for *s-trans* **7**<sub>VHF</sub> compared to *s-trans* **1**<sub>VHF</sub> at ca. 310 nm, which corresponds to a HOMO/LUMO(+1) transition. Both of these orbitals are in fact located exclusively on the 7-membered ring and this absorption could in fact coincide with the decreasing DHA absorption during the macrocyclic DHA-VHF to VHF-VHF isomerization. Thus, these two simultaneous processes could provide a rationale for why only a small absorptivity decrease is observed experimentally in the 350 nm region for this ring opening (Figure 8). Additionally, the spectral sum of an undisturbed *s-trans* **1**<sub>VHF</sub> chromophore and of the structurally distorted **7**<sub>VHF</sub> bears striking similarity to the spectrum attributed to the VHF-VHF state, lending further support to this hypothesis.

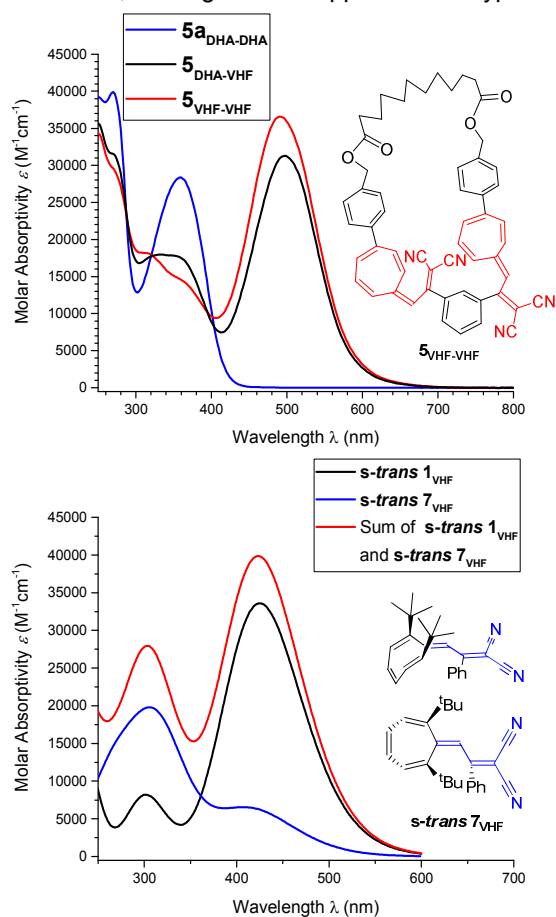


**Figure 8.** Top: Measured molar absorptivities of macrocycle **5** as a function of wavelength in MeCN. Bottom: Calculated molar absorptivities of *s-trans* **1**<sub>VHF</sub>, *s-trans* **7**<sub>VHF</sub><sup>10</sup>, and the sum of the two in MeCN (CAM-B3LYP/6-311+G(d,p) using the IEFPCM solvent model).

**Ring Closure Kinetics.** Thermal isomerizations were conducted for macrocycles **3**<sub>VHF-VHF</sub>, **4**<sub>VHF-VHF</sub>, and **5**<sub>VHF-VHF</sub> from VHF-VHF to DHA-VHF to DHA-DHA at 25, 40, 50, 60, 70 and 80 °C in MeCN. The kinetics of all thermal conversions were monitored by UV-Vis spectroscopy and observed to proceed in a stepwise manner via an initially fast decay followed by a slower one. The thermal

isomerization from **5**<sub>VHF-VHF</sub> to **5**<sub>DHA-VHF</sub> to **5**<sub>DHA-DHA a/b</sub> at 40 °C in MeCN is exemplified in Figure 9. Although theoretically, the isomerizations are complicated by several processes (*vide infra*), the decays monitored here could be quite accurately modeled by a sum of two exponential functions, assigned to the two thermal conversions shown in Scheme 3. Although this is an approximation, the assignment of each exponential to an individual VHF decay is reasonable due to the large differences in half-lives.

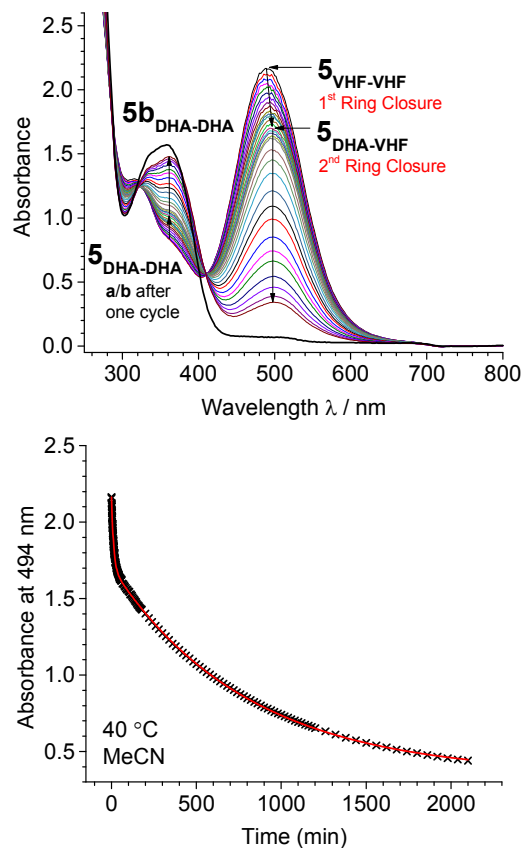


**Figure 9.** Top: Measured UV-Vis absorption spectra showing thermal conversion from **5**<sub>VHF-VHF</sub> to **5**<sub>DHA-VHF</sub> to **5**<sub>DHA-DHA a/b</sub> at 40 °C and the initial **5**<sub>DHA-DHA</sub> spectrum in MeCN. Measurements were conducted in a sealed ampule without baseline correction. Bottom: Absorbance at  $\lambda = 494$  nm plotted as a function of time and modeled by a sum of two exponential decay functions (red curve) using the expression  $A(t) = c_1 \exp(-k_{\text{fast}}t) + c_2 \exp(-k_{\text{slow}}t) + A_{\infty}$ .

Estimates of activation energies ( $E_a$ ) and pre-exponential factors ( $A$ ) for the two processes (VHF-VHF to DHA-VHF to DHA-DHA) were achieved using Arrhenius plots. In the same manner, Eyring plots (Figure 10) were used to estimate enthalpies ( $\Delta H^\ddagger$ ) and entropies ( $\Delta S^\ddagger$ ) of activation, from which Gibbs free energies of activation ( $\Delta G^\ddagger$ ) were calculated. It is notable that although the decay model achieves a great fit for the least strained macrocycle (**5**<sub>VHF-VHF</sub> to **5**<sub>DHA-VHF</sub> to **5**<sub>DHA-DHA</sub>), the fit somewhat worsens with increased strain. In fact, the slowest decay, which was recorded for **3**<sub>DHA-VHF</sub> to **3**<sub>DHA-DHA</sub> over 45 days at rt, exhibited a large enough deviation from the model that the initial and more sensitive decay from **3**<sub>VHF-</sub>

VHF to **3**<sub>DHA-VHF</sub> could not be reliably used in the calculation of kinetics parameters. This data point was thus not included in the Arrhenius or Eyring plots.

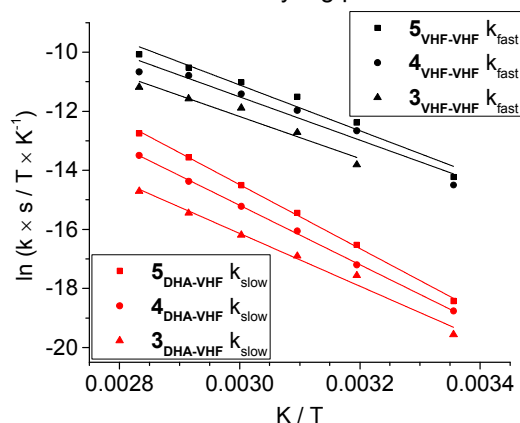


**Figure 10.** Eyring plots for the fast (VHF-VHF to DHA-VHF) and slow (DHA-VHF to DHA-DHA) thermal isomerization reactions of macrocycles **3**<sub>VHF-VHF</sub>, **4**<sub>VHF-VHF</sub>, and **5**<sub>VHF-VHF</sub>.

Thermodynamic parameters ( $E_a$ ,  $A$ ,  $\Delta H^\ddagger$ ,  $\Delta S^\ddagger$ ,  $\Delta G^\ddagger$ ) in addition to the rate constants ( $k$ ) and half-lives ( $t_{1/2}$ ) at room temperature for both the fast and slow thermal decay processes of the three macrocycles are summarized in Table 2. Comparing the rates of the two thermal ring closures as a function of macrocycle size and ring strain reveals that the ring closures systematically proceed slower (higher  $\Delta G^\ddagger$ s) with decreasing macrocycle size:  $5_{\text{VHF-VHF}} > 4_{\text{VHF-VHF}} > 3_{\text{VHF-VHF}}$ . Contrary to this, the enthalpies of activation ( $\Delta H^\ddagger$ ) for both the fast and slow thermal ring closure processes were actually found to decrease with decreasing macrocycle size. The observations of decreasing  $\Delta H^\ddagger$  but overall higher  $\Delta G^\ddagger$  values with decreasing macrocycle size can be reconciled by considering the entropy of activation ( $\Delta S^\ddagger$ ), which is revealed to progressively become more negative. The negative  $\Delta S^\ddagger$  values also suggest that entropy decreases upon forming the transition state, consistent with an associative, ring closing mechanism, generating a more ordered state. Secondly, progressively more negative  $\Delta S^\ddagger$  values with decreasing macrocycle size suggest that more conformational reorganization is needed for the smaller macrocycles to undergo ring closure than for the larger. Due to the fact that the larger macrocycles exhibit more degrees of freedom than the smaller, one VHF-to-DHA ring closure reaction will eliminate a greater proportion of degrees of freedom in the small cycles compared to the larger. For this reason, relatively greater reorganization, and thus larger  $\Delta S^\ddagger$  values, are observed in the smaller macrocycles, reflecting a higher energy requirement. Thus, the observation that the thermal ring closures are disfavored with decreasing macrocycle size can be rationalized by the fact that the increase in the entropic  $\Delta S^\ddagger$  contribution to the Gibbs free energy of activation ( $\Delta G^\ddagger$ ) outweighs the decreasing  $\Delta H^\ddagger$ . The overall result is a higher activation barrier ( $\Delta G^\ddagger$ ) in the smaller macrocycles. The thermal ring-closing isomerizations are, however, theoretically complicated by several other possible processes. Firstly, it should be noted that the second ring closure from DHA-VHF to DHA-DHA

proceeds to yield a pair of diastereoisomers which should, in principle, be theoretically modeled as two processes. Additionally, the *s-cis* / *s-trans* VHF equilibrium likely also plays a role, further slowing the thermal ring closure if the molecules cannot easily get from the usually more stable *s-trans* to the reactive *s-cis* conformation. In fact, this process can be used to explain the large difference between the first and second VHF-to-DHA ring closure rates. Structurally, the VHF-VHF states are thus hypothesized to present both a distorted VHF (close to *s-cis* based on computational results, *vide infra*) and an *s-trans* VHF moiety.

The isomerization from VHF to DHA may in principle proceed via two sites of ring closure, accessible by rotation about the exocyclic C3-C3a fulvene bond of VHF achievable via VHF *E/Z* isomerization. Consequently, the site of the linker bridging the two seven-membered rings can isomerize from the 7- to the 6-position in one or both of the DHA moieties of the DHA-DHA state. Previous reports on non-cyclic structures have indeed identified partial 7/6-isomerization to occur as a result of a light-heat cycle (ring-opening – ring-closure) yielding mixtures of two DHA isomers – evidenced by a significant redshift in the DHA absorption maxima.<sup>11</sup> The reaction rate model proposed here is only an approximation for two general reaction pathways, which we tentatively assign to an initially fast VHF-VHF to DHA-VHF ring closure followed by a slower DHA-VHF to DHA-DHA ring closure. Although the thermal reaction was not carried out to full completion in the experiment shown in Figure 9, it is clear that differences in the spectra are minimal. This reinforces our approximation that the thermal isomerization from VHF-VHF to DHA-DHA primarily proceeds to yield a diastereoisomeric mixture of **a/b** without any significant byproducts, which is also supported by TLC analysis.

**Calculations – Energy Landscape.** For a complete picture of the potential energy surface of the macrocyclic systems, a computational investigation was undertaken with the goal of providing estimates for macrocyclic geometries and relative energies between the DHA-DHA, DHA-VHF and VHF-VHF states of systems **3**, **4**, and **5**. A systematic conformer search was first carried out using a combination of the ConfGen program from MSTor<sup>11a</sup> and Gaussian 09<sup>11b</sup> to systematically generate a library of macrocyclic conformers.

	$k_{298\text{ K}}$ [ $10^{-5}\text{ min}^{-1}$ ]	$t_{1/2}$ [min]	$E_a$ [kJ mol $^{-1}$ ]	$A$ [ $10^8\text{ min}^{-1}$ ]	$\Delta H^\ddagger$ [kJ mol $^{-1}$ ]	$\Delta S^\ddagger$ [J K $^{-1}$ mol $^{-1}$ ]	$\Delta G^\ddagger_{298\text{ K}}$ [kJ mol $^{-1}$ ]
<b>3<sub>VHF-VHF</sub> → 3<sub>DHA-VHF</sub></b>	705	98	61.9	5.2	59.2	-121	95.3
<b>3<sub>DHA-VHF</sub> → 3<sub>DHA-DHA</sub></b>	5.7	12100	77.0	23	74.3	-109	106.7
<b>4<sub>VHF-VHF</sub> → 4<sub>DHA-VHF</sub></b>	905	77	63.7	19	61.0	-110	93.9
<b>4<sub>DHA-VHF</sub> → 4<sub>DHA-DHA</sub></b>	12.7	5460	86.4	1730	83.7	-72.8	105.4
<b>5<sub>VHF-VHF</sub> → 5<sub>DHA-VHF</sub></b>	1180	59	67.1	99	64.4	-97.5	93.5
<b>5<sub>DHA-VHF</sub> → 5<sub>DHA-DHA</sub></b>	17.8	3900	92.7	34200	89.5	-49.5	104.2

**Table 2. Experimentally determined thermodynamic parameters for the first (VHF-VHF to DHA-VHF) and second (DHA-VHF to DHA-DHA) thermal isomerizations of macrocycles 3<sub>VHF-VHF</sub>, 4<sub>VHF-VHF</sub>, and 5<sub>VHF-VHF</sub>.**

Due to the cyclic structure of the macrocycles, bonds could not be freely rotated and were therefore broken to achieve rotation. Two- and three-fold rotations about single bonds were allowed according to Figure S23 (see SI). The original connectivity was then re-imposed in Gaussian 09 and a force-field (Dreiding) optimization was run on each conformer to generate more than 1.3 million macrocyclic structures. Conformers presenting interatomic distances of less than 0.5 Å were automatically discarded by the MSTor program. For all macrocycles **3**, **4**, and **5**, the 100 lowest energy conformers of each DHA/VHF subunit orientation were subjected to PM3 geometry optimizations and frequency calculations. This corresponds to 600 DHA-DHA (300 **a** / 300 **b**), 800 DHA-VHF, and 1000 VHF-VHF conformers. The SI contains more details for the conformer selection procedures. The number of conformers used to proceed with is representative of the various DHA and VHF conformations that are accessible by the macrocycles, not to conformational variations in the alkyl bridge. Thus, fewer “characteristic” DHA-DHA conformers are required to achieve a representative sample of the conformational energy landscape as this state is much more rigid than the systems including VHF moieties. Notably, PM3 optimization results indicate that the relative energy differences between the lowest energy conformers of the DHA-DHA, DHA-VHF, and VHF-VHF macrocycles are very precise representations of the energy differences considering a distribution (90% Boltzmann weighted average) of the lowest energy conformers of each state (See SI for details). Additionally, PM3-calculated relative energies ( $\Delta G$ ) also predict a correct energetic stability trend between the macrocycles, that is,  $\Delta G$  DHA-DHA < DHA-VHF < VHF-VHF.

To obtain more accurate Gibbs free energies ( $\Delta G$ ), selected PM3-optimized structures were subjected to M06-2X/6-31+G(d) geometry optimizations and frequency calculations in vacuum. The lowest-energy conformers and relative energies are presented in Figure 11. Ener-

gies of other “characteristic” conformers are provided in SI (Table S8).

The results obtained from DFT geometry optimizations seem to provide reasonably accurate structural representations for the individual DHA/VHF chromophoric units (Figure 11). This is judged on the basis of experimental UV-Vis absorption spectra, which correlate well with the conformations of these chromophores. For all macrocyclic systems, the DHA-DHA state presents two relatively undistorted core DHA chromophores. Similarly, all lowest-energy DHA-VHF systems present the hypothesized undistorted DHA moiety as well as the planar and undistorted *s-trans* VHF moiety. Lastly and again according to hypothesis, all lowest-energy macrocyclic VHF-VHF conformers exhibit a planar, *s-trans* VHF as well as a partially out-of-plane, *s-cis* VHF moiety. These observations not only explain the characteristic UV-Vis absorption spectra assigned to these states (*s-trans* VHF and distorted VHF of VHF-VHF) but also the initially fast VHF-VHF to DHA-VHF thermal isomerization (distorted VHF is close to an *s-cis* conformation) and the subsequently slow DHA-VHF to DHA-DHA reaction (from the *s-trans* VHF).

The calculated lowest-energy conformers for the macrocyclic DHA-VHF and VHF-VHF systems are all found to exhibit “ring-collapsed” structures to various degrees (characterized by reduced cavity space). This is a reasonable consequence of simulating structural optimizations in vacuum without explicit solvent molecules. As the rigid DHA-DHA macrocycles maintain an open structure, a relative energy comparison between these and the ring-collapsed DHA-VHF or VHF-VHF macrocycles is unfounded. In fact, the relative Gibbs free energies ( $\Delta G$ ) between the DHA-DHA and DHA-VHF macrocycles seem unreasonable, as the data suggest a more stable DHA-VHF than DHA-DHA for **3** and **4**, contradictory to experimental observations, which reveal DHA-DHA to be thermodynamically most favorable at 25 °C (as >75% DHA-DHA seemed to have formed from DHA-VHF when the experiment was stopped, and the ultraslow conver-

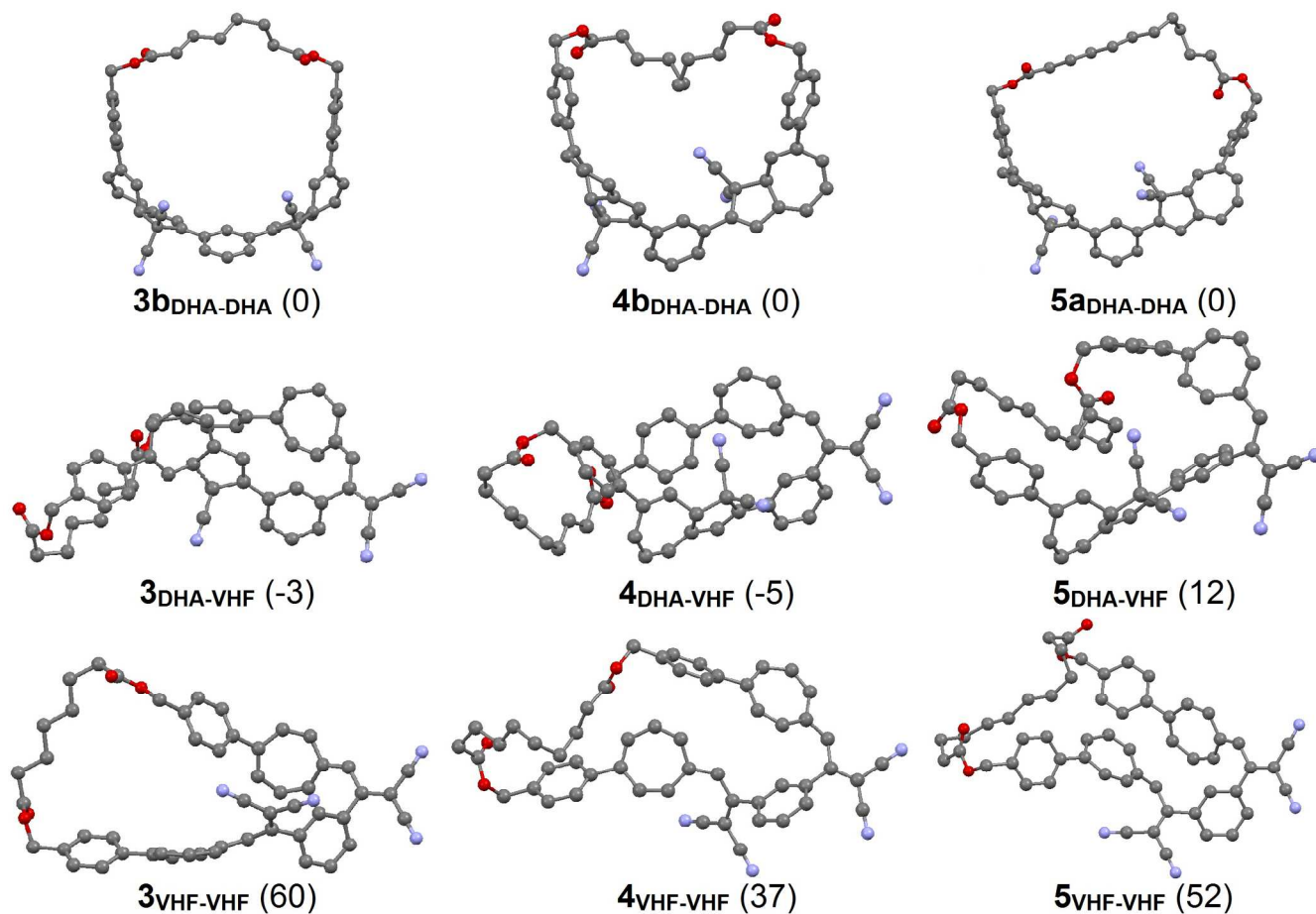
1 sion was clearly not complete at this stage). Solvation  
2 would likely have a larger stabilizing influence on the  
3 DHA-DHA isomer than on the more flexible DHA-VHF  
4 and VHF-VHF isomers for which favorable intramolecu-  
5 lar van der Waals interactions are already present in the  
6 gas phase structures. Thus, in solution, the DHA-VHF  
7 and VHF-VHF states will likely be more energetic relative  
8 to the DHA-DHA state than in the gas phase. Optimiza-  
9 tions involving solvent modeling or guest molecules  
10 occupying the macrocyclic cavities perhaps using  
11 QM/MM methods<sup>12</sup> might provide more accurate estima-  
12 tions of the relative energy differences. Nevertheless,  
13 considering the lowest-energy DHA-DHA and VHF-VHF  
14 conformers in the gas phase (Figure 11), we see that the  
15 smallest, most strained macrocycle **3** clearly exhibits the  
16 most energetic VHF-VHF state: 60 kJ mol<sup>-1</sup> (**3**<sub>VHF-VHF</sub>).  
17 This corresponds to 30 kJ per mole VHF. This value is  
18 similar to the parent system **1** (28 kJ mol<sup>-1</sup>), but since the  
19 gas phase VHF-VHF structure is more collapsed than  
20 the DHA-DHA structure, it is expected that solvation  
21 would in actual fact result in an increased energy storage  
22 of the macrocycle. Notably, the largest macrocycle **5** has  
23 a more energetic VHF-VHF state than **4** in the gas  
24 phase, so a general correlation between ring size and  
25 energy density is more complicated.

## 25 Conclusion

26 The switching properties of two *meta*-phenylene-bridged  
27 DHA units can be finely tuned by incorporation into mac-  
28 rocyclic structures of various sizes. Thus, we find that  
29 cyclization causes step-wise, photoinduced ring opening  
30 reactions to the VHF-VHF isomer and subsequent step-  
31 wise thermal ring closure reactions. Particularly interest-  
32 ing, we were able to tune the half-life of the second VHF  
33 ring closure reaction (DHA-VHF to DHA-DHA) in the  
34 macrocycles from 65 h (**5**) to 91 h (**4**) to 202 h (**3**) at  
35 room temperature by decreasing the macrocyclic ring  
36 size. The hampering of the second VHF ring closure  
37 reaction seems in particular to be the result of an unfav-  
38 orable entropic term, increasing with increased ring  
39 strain. By combining the current macrocyclic approach  
40 with other structural modifications, it may be possible to  
41 set the back reaction completely on stand-by. For ulti-  
42 mate release of the energy when needed, we may em-  
43 ploy our recent discovery that the back reaction is pro-  
44 moted by the action of Cu(I) ions.<sup>13</sup> We are currently also  
45 targeting other triggering mechanisms. Indeed, a fast  
46 thermal discharge upon activation is needed in order for  
47 a MOST system to deliver high power.

48 It is more difficult to find a correlation between ring size  
49 and energy density, at least based on the gas phase  
50 structures reported in this work. Yet, the smallest macro-  
51 cycle in the series has the largest energy difference  
52 between DHA-DHA and VHF-VHF states. For increasing  
53 the overall energy density of the system, low-energy,  
54 ring-collapsed conformers should ideally be avoided.  
55 Collapses are likely avoided by solvation or by incorpo-  
56 rating the macrocycles in mechanically interlocked struc-  
57 tures, such as rotaxanes and catenanes.<sup>6c,14</sup> Such strat-  
58 egies could reveal the further assets of photoswitchable  
59 macrocycles and should certainly be the scope of future  
60

investigations, not only for advancing MOST systems but  
in general for development of smart functional materials.



31 **Figure 11.** Calculated (M06-2X/6-31+G(d)) lowest-energy conformations of macrocycles **3**, **4**, and **5** and Gibbs free energies  
 32 ( $\Delta G/\text{kJ mol}^{-1}$ ; in brackets) relative to the lowest-energy DHA-DHA conformers. Hydrogen atoms were removed for clarity. For  
 33 reference system  $1_{\text{DHA}}/s\text{-trans } 1_{\text{VHF}}$ ,  $\Delta G = 28 \text{ kJ mol}^{-1}$ .

### 34 Experimental Section

35  
 36 **General Methods.** All light-sensitive compounds, reactions and manipulations were shielded from light by either  
 37 conducting the procedures in a dimly lit room or by masking the glassware and equipment with aluminum  
 38 foil. Common solvents were dried, distilled, and degassed prior to use as follows:  $\text{CH}_2\text{Cl}_2$  was dried using a  
 39 solvent purification system;  $\text{CH}_2\text{Cl}_2$  was alternatively dried over 3 Å molecular sieves. Commercially available  
 40 reagents including 4-dimethylaminopyridine (DMAP), suberoyl chloride, and dodecanedioyl dichloride were  
 41 purchased from commercial sources and used as received without further purification. 2,2'-(1,3-  
 42 Phenylene)bis(7-(4-(hydroxymethyl)phenyl)azulene-1,1(8a*H*)-dicarbonitrile) (**6**) was synthesized with only  
 43 partial purification, according to literature procedure.<sup>3b</sup>  
 44 Purification of products carried out by flash column chromatography was conducted using silica gel (60 Å  
 45 pore size; 43-60 μm particle size). Nuclear magnetic resonance (NMR) spectra were acquired on either a  
 46 500-MHz instrument ( $^1\text{H}$  at 500 MHz,  $^{13}\text{C}$  at 126 MHz) equipped with a non-inverse cryo probe or a penta-  
 47 probe/broad-band probe. Chemical shift values are provided relative to internal solvent references for  $^1\text{H}$  and  
 48  $^{13}\text{C}$ -NMR spectra. Infrared spectroscopy (IR) data were

acquired on an ATR single reflection diamond instrument. Samples were loaded directly or by evaporation  
 from a suitable solvent. IR absorptions are reported in units of wavenumbers ( $\text{cm}^{-1}$ ). Mass spectra were recorded  
 by using a MALDI-FT-ICR instrument equipped with a 7 T magnet (prior to the experiments, the instrument was  
 calibrated using sodium trifluoroacetate ( $\text{NaTFA}$ ) cluster ions). Thin layer chromatography (TLC) was conducted  
 using commercially available, precoated plates (silica 60) with fluorescence indicator. With respect to the DHA  
 compounds, TLC was carried out in the absence of light; a color change from yellow to red upon exposure to UV  
 light indicates a conversion to VHF. Size exclusion column chromatography was conducted on S-X8 polystyrene  
 biobeads using  $\text{CH}_2\text{Cl}_2$  as eluent. All melting points are uncorrected.

49  
 50 **General Macrocyclization Reaction Procedure.** A flame-dried, 3-necked, 250 mL rbf was equipped with  
 51 two 50 mL dropping funnels and charged with a solution of 4-dimethylaminopyridine (76 mg, 0.62 mmol) in dry  
 52  $\text{CH}_2\text{Cl}_2$  (40 mL) under  $\text{N}_2$  atmosphere. The dropping funnels were loaded with two solutions of i) di-acid chloride  
 53 (suberoyl chloride or dodecanedioyl dichloride) (0.19 mmol) in  $\text{CH}_2\text{Cl}_2$  (40 mL) and ii) compound **6** (100 mg,  
 54 0.16 mmol). The contents of the dropping funnels were then added dropwise to the reaction vessel over 30 min,

and the reaction mixture was stirred at rt for another 3.5 h in the absence of light. The reaction mixture was transferred to a separatory funnel and washed with 1 M HCl (2 x 50 mL) followed by H<sub>2</sub>O (50 mL). The organic phase was isolated, dried over MgSO<sub>4</sub>, filtered, and concentrated *in vacuo*. The residue was purified by flash column chromatography (SiO<sub>2</sub>, 1% AcOH/toluene) to isolate the two diastereoisomers of the title compounds with minor azulene impurities. The mixtures were further purified by size exclusion column chromatography on S-X8 polystyrene biobeads using CH<sub>2</sub>Cl<sub>2</sub> as eluent. The products could be concentrated from a mixture of CH<sub>2</sub>Cl<sub>2</sub>/heptanes to yield the title compounds as well-behaved yellow solids.

**3a:** pale yellow solid (7 mg, 6%). Stereochemistry was assigned as the complementary diastereoisomer to **3b**. TLC (40% EtOAc/toluene)  $R_f = 0.81$ . Mp: 120-140 °C darkens to a red/orange solid, 150 - 155 °C melts to red/orange liquid. <sup>1</sup>H NMR (500 MHz, CDCl<sub>3</sub>) δ 7.91 (br t,  $J = 1.7$  Hz, 1H), 7.77 (dd,  $J = 7.9, 1.7$  Hz, 2H), 7.60 (t,  $J = 7.9$  Hz, 1H), 7.34 (d,  $J_{AB} = 8.3$  Hz, 4H), 7.31 (d,  $J_{AB} = 8.3$  Hz, 4H), 6.89 – 6.79 (m, 6H), 6.40 (br d,  $J = 5.5$  Hz, 2H), 5.80 (d,  $J = 4.8$  Hz, 2H), 5.11 (d,  $J_{AB} = 12.2$  Hz, 2H), 5.07 (d,  $J_{AB} = 12.2$  Hz, 2H), 3.80 (dd,  $J = 4.8, 1.2$  Hz, 2H), 2.29 – 2.24 (m, 4H), 1.60 – 1.55 (m, 4H), 1.29 – 1.25 (m, 4H) ppm. <sup>13</sup>C NMR (126 MHz, CDCl<sub>3</sub>) δ 173.4, 140.7, 140.0, 139.2, 138.6, 136.4, 133.4, 132.7, 132.4, 131.6, 130.4, 128.9, 127.9, 127.9, 126.0, 120.9, 117.5, 115.1, 113.0, 65.7, 51.0, 45.9, 34.6, 29.3, 25.0 ppm. IR: 3031w, 2928m, 2856m, 2252w, 1732s, 1655m, 1612w, 1567w, 1513m, 1487m, 1454m, 1413m, 1370m, 1292m, 1244m, 1213m cm<sup>-1</sup>. HRMS (MALDI+ FT-ICR, Dithranol,  $m/z$ ): found 785.31391 [M+H]<sup>+</sup>, calc. for [C<sub>52</sub>H<sub>41</sub>N<sub>4</sub>O<sub>4</sub>]<sup>+</sup> 785.31223 [M+H]<sup>+</sup>.

**3b:** pale yellow solid (8 mg, 7%). Crystals suitable for X-ray diffraction were grown from layered CHCl<sub>3</sub>/heptane which was also used to determine stereochemistry. TLC (40% EtOAc/toluene)  $R_f = 0.77$ . Mp: 120-140 °C darkens to a red/orange solid, 156 - 163 °C melts to red/orange liquid. <sup>1</sup>H NMR (500 MHz, CDCl<sub>3</sub>) δ 7.83 (dd,  $J = 7.9, 1.1$  Hz, 2H), 7.68 (t,  $J = 7.9$  Hz, 1H), 7.59 (br t,  $J = 1.1$  Hz, 1H), 7.33 (d,  $J_{AB} = 8.3$  Hz, 4H), 7.30 (d,  $J_{AB} = 8.3$  Hz, 4H), 6.86 (dd,  $J = 11.4, 5.5$  Hz, 2H), 6.81 (d,  $J = 11.4$  Hz, 2H), 6.71 (s, 2H), 6.33 (br d,  $J = 5.5$  Hz, 2H), 5.78 (d,  $J = 4.8$  Hz, 2H), 5.08 (d,  $J_{AB} = 12.1$  Hz, 2H), 5.04 (d,  $J_{AB} = 12.1$  Hz, 2H), 3.79 (d,  $J = 4.8$  Hz, 2H), 2.26 – 2.20 (m, 4H), 1.53 – 1.49 (m, 4H), 1.26 – 1.21 (m, 4H) ppm. <sup>13</sup>C NMR (126 MHz, CDCl<sub>3</sub>) δ 173.4, 141.6, 139.8, 138.9, 138.5, 136.4, 132.9, 132.8, 132.6, 131.6, 130.5, 129.1, 127.9, 127.5, 126.9, 120.5, 117.5, 115.1, 112.7, 65.8, 51.3, 45.8, 34.5, 29.1, 24.8 ppm. IR: 3058w, 3027w, 2929m, 2861m, 2250w, 1732s, 1654m, 1612w, 1513m, 1487m, 1455m, 1410m, 1368m, 1291m, 1260m, 1214m cm<sup>-1</sup>. HRMS (MALDI+ FT-ICR, Dithranol,  $m/z$ ): found 785.31391 [M+H]<sup>+</sup>, calc. for [C<sub>52</sub>H<sub>41</sub>N<sub>4</sub>O<sub>4</sub>]<sup>+</sup> 785.31223 [M+H]<sup>+</sup>.

**4a:** pale yellow solid (10 mg, 8%). Characterization data are consistent with those previously reported.<sup>3b</sup>

**4b:** pale yellow solid (11 mg, 9%). Characterization data are consistent with those previously reported.<sup>3b</sup>

**5a:** pale yellow solid (17 mg, 13%). Crystals suitable for X-ray diffraction were grown from layered CHCl<sub>3</sub>/EtOH which was also used to determine stereochemistry. TLC (40% EtOAc/toluene)  $R_f = 0.84$ . Mp: 120 °C darkens to orange solid, 131 - 136 °C melts to orange liquid. <sup>1</sup>H NMR (500 MHz, CDCl<sub>3</sub>) δ 7.97 (t,  $J = 1.7$  Hz, 1H), 7.80 (dd,  $J = 7.9, 1.7$  Hz, 2H), 7.61 (t,  $J = 7.9$  Hz, 1H), 7.38 (br d,  $J_{AB} = 8.4$  Hz, 4H), 7.34 (br d,  $J_{AB} = 8.4$  Hz, 4H), 6.94 (s, 2H), 6.87 (dd,  $J = 11.5, 5.8$  Hz, 2H), 6.81 (d,  $J = 11.5$  Hz, 2H), 6.43 (br d,  $J = 5.8$  Hz, 2H), 5.91 (d,  $J = 4.8$  Hz, 2H), 5.12 (d,  $J_{AB} = 12.3$  Hz, 2H), 5.08 (d,  $J_{AB} = 12.3$  Hz, 2H), 3.83 (dd,  $J = 4.8, 1.3$  Hz, 2H), 2.30 – 2.26 (m, 4H), 1.60 – 1.55 (m, 4H), 1.27 – 1.18 (m, 12H) ppm. <sup>13</sup>C NMR (126 MHz, CDCl<sub>3</sub>) δ 173.6, 140.3, 139.9, 139.3, 139.2, 136.4, 133.0, 132.8, 132.0, 131.9, 130.4, 128.8, 128.0, 127.5, 124.5, 121.1, 117.1, 115.3, 112.9, 65.7, 51.0, 45.2, 34.7, 29.9, 29.7, 29.5, 25.1 ppm. IR: 3031w, 2926m, 2854m, 2254w, 2208w, 1730m, 1609w, 1513w, 1486w, 1455w, 1379w, 1350w, 1244m, 1216m cm<sup>-1</sup>. HRMS (MALDI+ FT-ICR, Dithranol,  $m/z$ ): found 841.37592 [M+H]<sup>+</sup>, calc. for [C<sub>56</sub>H<sub>49</sub>N<sub>4</sub>O<sub>4</sub>]<sup>+</sup> 841.37483 [M+H]<sup>+</sup>.

**5b:** pale yellow solid (21 mg, 16%). Crystals were grown from layered CHCl<sub>3</sub>/heptanes and CHCl<sub>3</sub>/EtOH but neither were suitable for X-ray diffraction. Stereochemistry was assigned as the complementary diastereoisomer to **5a**. TLC (40% EtOAc/toluene)  $R_f = 0.78$ . Mp: 120 °C darkens to orange solid, 128 - 134 °C melts to orange liquid. <sup>1</sup>H NMR (500 MHz, CDCl<sub>3</sub>) δ 7.95 (t,  $J = 1.8$  Hz, 1H), 7.83 (dd,  $J = 7.9, 1.8$  Hz, 2H), 7.64 (t,  $J = 7.9$  Hz, 1H), 7.37 (br d,  $J_{AB} = 8.4$  Hz, 4H), 7.33 (br d,  $J_{AB} = 8.4$  Hz, 4H), 6.88 (s, 2H), 6.84 (dd,  $J = 11.5, 5.6$  Hz, 2H), 6.80 (d,  $J = 11.5$  Hz, 2H), 6.38 (br d,  $J = 5.6$  Hz, 2H), 5.94 (d,  $J = 4.8$  Hz, 2H), 5.10 (s, 4H), 3.85 (dd,  $J = 4.8, 1.5$  Hz, 2H), 2.31 – 2.27 (m, 4H), 1.60 – 1.53 (m, 4H), 1.26 – 1.17 (m, 12H) ppm. <sup>13</sup>C NMR (126 MHz, CDCl<sub>3</sub>) δ 173.7, 140.8, 139.8, 139.4, 139.2, 136.5, 132.9, 132.6, 132.1, 132.1, 130.5, 128.7, 128.0, 127.6, 125.0, 120.9, 117.0, 115.0, 112.7, 65.7, 51.1, 45.4, 34.7, 29.8, 29.6, 29.5, 25.1 ppm. IR: 3061w, 3029w, 2926m, 2854m, 2255w, 2207w, 1730m, 1611w, 1513w, 1442w, 1417w, 1378w, 1351w, 1246m, 1217m cm<sup>-1</sup>. HRMS (MALDI+ FT-ICR, Dithranol,  $m/z$ ): found 841.37727 [M+H]<sup>+</sup>, calc. for [C<sub>56</sub>H<sub>49</sub>N<sub>4</sub>O<sub>4</sub>]<sup>+</sup> 841.37483 [M+H]<sup>+</sup>.

## AUTHOR INFORMATION

### Corresponding Author

\* E-mail: mbn@chem.ku.dk

### Author Contributions

The manuscript was written through contributions of all authors.

### Funding Sources

We thank University of Copenhagen for supporting this work.

## ASSOCIATED CONTENT

### Supporting Information

The Supporting Information is available free of charge on the ACS Publications website at DOI: ###.

NMR/IR/UV-Vis spectra, switching studies, computational data, X-ray crystallographic data (PDF)

X-ray crystallographic data for **3b**<sub>DHA-DHA</sub> (CIF)

X-ray crystallographic data for **5a**<sub>DHA-DHA</sub> (CIF)

## REFERENCES

1. (a) Tian, H.; Yang, S. *J. Chem. Soc. Rev.* **2004**, *33*, 85-97; (b) Russew, M.-M.; Hecht, S. *Adv. Mater.* **2010**, *22*, 3348-3360; (c) Irie, M.; Fukaminato, T.; Matsuda, K.; Kobatake, S. *Chem. Rev.* **2014**, *114*, 12174-12277; (d) Zhang, J.; Zhou, Q.; Tian, H. *Adv. Mater.* **2012**, *25*, 378-399; (e) Szymáński, W.; Beierle, J. M.; Kistemaker, H. A.; Veleva, W. A.; Feringa, B. L. *Chem. Rev.* **2013**, *113*, 6114-6178; (f) Broman, S. L.; Nielsen, M. B. *Phys. Chem. Chem. Phys.* **2014**, *16*, 21172-21182.

2. (a) Daub, J.; Knöchel, T.; Mannschreck, A. *Ang. Chem. Int. Ed. Engl.* **1984**, *23*, 960-961; (b) Görner, H.; Fischer, C.; Gierisch, S.; Daub, J. *J. Phys. Chem.* **1993**, *97*, 4110-4117.

3. (a) Olsen, S. T.; Elm, J.; Storm, F. E.; Gejl, A. N.; Hansen, A. S.; Hansen, M. H.; Nikolajsen, J. R.; Nielsen, M. B.; Kjaergaard, H. G.; Mikkelsen, K. V. *J. Phys. Chem. A* **2015**, *119*, 896-904; (b) Vlasceanu, A.; Broman, S. L.; Hansen, A. S.; Skov, A. B.; Cacciarini, M.; Kadziola, A.; Kjaergaard, H. G.; Mikkelsen, K. V.; Nielsen, M. B. *Chem. Eur. J.* **2016**, *22*, 10796-10800.

4. (a) Yoshida, Z.-I. *J. Photochem.* **1985**, *29*, 27-40; (b) Kanai, Y.; Srinivasan, V.; Meier, S. K.; Vollhardt, K. P. C.; Grossman, J. C. *Angew. Chem. Int. Ed.* **2010**, *49*, 8926-8929; (c) Kucharski, T. J.; Tian, Y.; Akbulatov, S.; Boulatov, R. *Energy Environ. Sci.* **2011**, *4*, 4449-4472; (d) Durgun, E.; Grossman, J. C. *J. Phys. Chem. Lett.* **2013**, *4*, 854-860; (e) Kucharski, T. J.; Ferralis, N.; Kolpak, A. M.; Zheng, J. O.; Nocera, D. G.; Grossman, J. C. *Nature Chem.* **2014**, *6*, 441-447; (f) Lennartson, A.; Roffey, A.; Moth-Poulsen, K. *Tetrahedron Lett.* **2015**, *56*, 1457-1465; and references cited therein; (g) Dreos, A.; Börjesson, K.; Wang, Z.; Roffey, A.; Norwood, Z.; Kushnir, D.; Moth-Poulsen, K. *Energy Environ. Sci.* **2017**, *10*, 728-734.

5. Broman, S. L.; Brand, S. L.; Parker, C. R.; Petersen, M. Å.; Tortzen, C. G.; Kadziola, A.; Kilså, K.; Nielsen, M. B. *ARKIVOC* **2011**, *ix*, 51-67.

6. For examples of macrocycles incorporating azobenzenes, see: (a) Norikane, Y.; Tamaoki, N. *Org. Lett.* **2004**, *6*, 2595-2598; (b) Bassotti, E.; Carbone, P.; Credi, A.; Di Stefano, M.; Masiero, S.; Negri, F.; Orlandi, G.; Spada, G. P. *J. Phys. Chem. A* **2006**, *110*, 12385-12394; (c) Uchida, E.; Sakaki, K.; Nakamura, Y.; Azumi, R.; Hirai, Y.; Akiyama, H.; Yoshida, M.; Norikane, Y. *Chem. Eur. J.* **2013**, *19*, 17391-17397; (d) Schweighauser, L.; Häussinger, D.; Neuburger, M.; Wegner, H. A. *Org. Biomol. Chem.* **2014**, *12*, 3371-3379.

7. Evans, M. G.; Polanyi, M., *J. Chem. Soc., Faraday Trans.* **1936**, *32*, 1333-1360.

8. Petersen, A. U.; Broman, S. L.; Olsen, S. T.; Hansen, A. S.; Du, L.; Kadziola, A.; Hansen, T.; Kjaergaard, H. G.; Mikkelsen, K. V.; Nielsen, M. B. *Chem. Eur. J.* **2015**, *21*, 3968-3977.

9. For relationships between ring size, yield, and melting points of cycloalkane and other macrocycles, see for example: Dale, J. *J. Chem. Soc.* **1963**, 93-111.

10. Lubrin, N. C. M.; Vlasceanu, A.; Frandsen, B. N.; Skov, A. B.; Kilde, M. D.; Mikkelsen, K. V.; Nielsen, M. B. *Eur. J. Org. Chem.* **2017**, 2932-2939.

11. (a) Zheng, J.; Mielke, S. L.; Clarkson, K. L.; Truhlar, D. G. *Comput. Phys. Commun.* **2012**, *183*, 1803-1812; (b) Frisch, M. J. *et al.*, Gaussian, Inc., Wallingford CT, **2013**.

12. (a) Poulsen, T. D.; Ogilby, P. R.; Mikkelsen, K. V. *J. Chem. Phys.* **2001**, *115*, 7843-7851; (b) Kongsted, J.; Osted, A.; Mikkelsen, K. V.; Astrand, P.-O.; Christiansen, O. *J. Chem. Phys.* **2004**, *121*, 8435-8445.

13. (a) Cacciarini, M.; Vlasceanu, A.; Jevric, M.; Nielsen, M. B. *Chem. Commun.* **2017**, *53*, 5874-5877; (b) Wang, Z.; Udmark, J.; Börjesson, K.; Rodrigues, R.; Abrahamsson, M.; Nielsen, M. B.; Moth-Poulsen, K. *ChemSusChem* **2017**, *10*, 3049-3055.

14. Shilova, E. A.; Perevalov, V. P.; Suslov, V. V.; Moustrou, C.; *Tetrahedron Lett.* **2008**, *49*, 3453-3457.

